Conf-9204106--4

MELT COOLABILITY MODELING AND COMPARISON TO MACE TEST RESULTS

M. T. Farmer, J. J. Sienicki and B. W. Spencer

Argonne National Laboratory
Argonne, Illinois 60439 USA

ANL/CP--75620

DE92 010506

ABSTRACT

An important question in the assessment of severe accidents in light water nuclear reactors is the ability of water to quench a molten corium-concrete interaction and thereby terminate the accident progression. As part of the Melt Attack and Coolability Experiment (MACE) Program, phenomenological models of the corium quenching process are under development. The modeling approach considers both bulk cooldown and crust-limited heat transfer regimes, as well as criteria for the pool thermal hydraulic conditions which separate the two regimes. The model is then compared with results of the MACE experiments.

INTRODUCTION

Under certain severe accident sequences in current light water nuclear reactors, molten core material (corium) is postulated to breach the lower head of the reactor pressure vessel and relocate downward onto the concrete basemat of the containment building. In the absence of water, the subsequent molten corium-concrete interaction (MCCI) will lead to gas, aerosol, and fission product release into the containment atmosphere. A critical question to be addressed in these ex-vessel accident sequences is the ability of water introduced atop the MCCI to quench the corium and thereby terminate the accident progression.

When water is introduced atop an MCCI, several coolability sequences may be envisioned, depending upon the MCCI initial conditions. An illustration of a potential melt coolabilty flow diagram is shown in Figure 1. In the short term following water addition, the question of whether or not a significant amount of the melt thermal energy is removed may depend upon whether or not a stable crust is able to form which would then inhibit heat transfer from the MCCI region to the water layer. For a stable crust to form over an MCCI, it is envisioned that

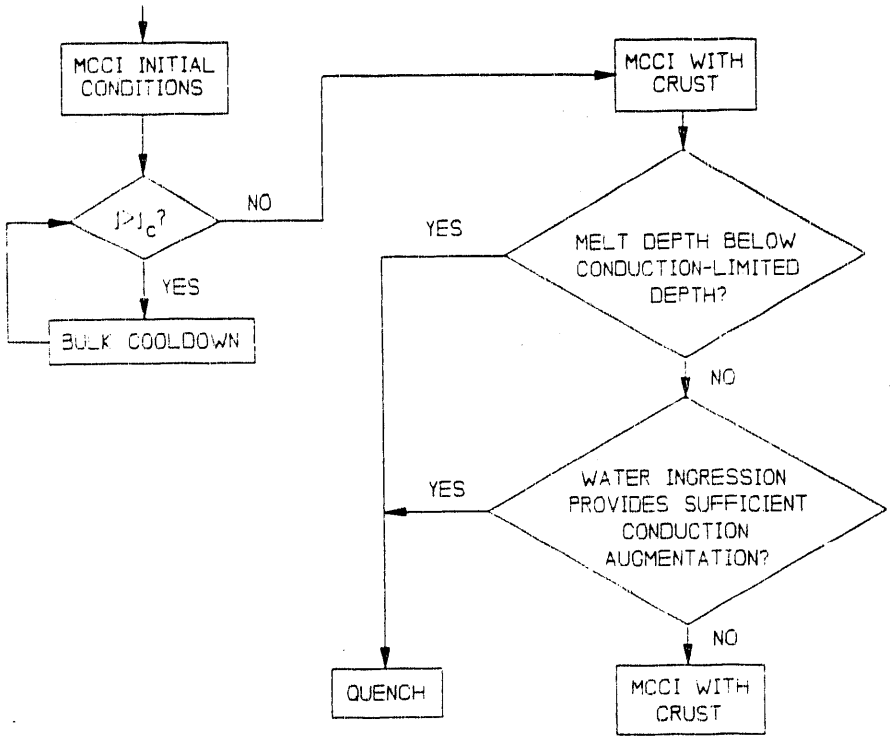

Figure 1. Illustration of a potential melt coolability flow diagram.

two necessary conditions must be met: (i) a thermal condition, viz., the melt/water interfacial temperature must fall below the corium freezing temperature, and (ii) a mechanical condition, viz., the incipient crust must be stable with respect to local mechanical loads imposed by the agitated melt. If either of these two conditions is violated, then stable crust formation at the interface between the MCCI zone and water layer may be precluded. In this regime, film boiling is expected to be the dominant heat transfer mode due to periodic introduction of high temperature melt at the interface as the crust segments are broken up. Efficient melt/water heat transfer may thus be anticipated owing to conduction and, predominately, radiation heat transfer across the agitated (i.e., area enhanced) melt/water interface, in addition to the possible entrainment of melt droplets into the water overlayer. In a purely bulk freezing heat transfer mode, frozen material formed at the interface will be mixed back into the melt causing an overall decline in the bulk melt temperature, and eventually lead to the development of a slurry mixture.

As the bulk cooling heat transfer mode continues, the melt temperature will gradually decline. If the downward heat transfer rate, which drives concrete ablation with concurrent noncondensable gas release, is proportional to melt temperature, then the melt sparging rate will also decrease. Thus, a point may be reached at which the thermal and mechanical thresholds for interfacial crust formation are both satisfied and an insulating crust forms between the coherent melt zone and water layer. The physical configuration at this point would consist of an ongoing MCCI zone at reduced temperature with a crust atop the melt. Cooling of the melt zone would then be limited by conduction through the crust. The crust will be characterized by some degree of porosity, or cracks, owing to the necessity of venting concrete decomposition gases. Thus, the possibility exists for enhanced cooling of the MCCI zone via water ingression through the crust perforations. After the crust is formed, quench will eventually be achieved if one of the following two conditions is met: (i) melt depth lies below the minimum depth at which decay heat can be removed via conduction alone, or (ii) water ingression through cracks/crevices within the crust provides sufficient conduction augmentation to remove the decay heat source.

As part of the Melt Attack and Coolability Experiment (MACE) program at ANL, phenomenological models are being developed to study the melt/water/concrete interaction process. A first order Corium Quenching (CORQUENCH) film boiling heat transfer model has been developed (1), which considers the affects of conduction and radiation heat transfer across the vapor film, bulk coolant subcooling, and interfacial area enhancement due to sparging concrete decomposition gases. This model is currently limited to the bulk cooling regime in which mixing associated with sparging gases is sufficient to preclude stable interfacial crust formation (1). The current paper describes the extension of the CORQUENCH model to treat both the bulk cooling and crust-limited heat transfer regimes. The approach is to define appropriate thermal/mechanical thresholds for incipient crust growth at the melt/water interface. Below these thresholds, the original CORQUENCH film boiling model (1) is embodied in a full boiling curve to treat quenching behavior of the crust upper surface. The current work focuses on the case in which heat transfer from the MCCI zone is limited by conduction through the crust; i.e., no treatment of water ingression phenomena is provided here. The modified version of the CORQUENCH model is then compared

to the results of MACE scoping test (2).

MODEL DEVELOPMENT

To assess the potential for crust formation over an MCCI with water present, expressions are required for the thermal and mechanical crust stability limits. The thermal condition for inception of crust growth at the melt/water interface is that the interfacial temperature, in the absence of a crust, must fall below the melt freezing temperature. The energy balance at the interface is of the form,

$$h_w (T_I - T_{sat}) = h_m (T_m - T_I), \tag{1}$$

where T_m melt temperature, T_I = melt/water interfacial temperature, T_{sat} = water saturation temperature, h_w = heat transfer coefficient to water, and h_m = melt convective heat transfer coefficient to the underside of the crust. The thermal criterion for inception of crust growth is that the interface temperature, as determined from Eq. 1, must satisfy the condition,

$$T_I < T_f \tag{2}$$

where T_f = melt freezing temperature. The melt convective heat transfer coefficient is evaluated using Kutateladze's bubble agitation heat transfer coefficient (3), which is given through the equation

$$h_m = \begin{cases} 1.5 \cdot 10^{-3} \left(\frac{k_m}{L}\right) \left(\frac{Pc_m j_g}{k_m g}\right)^{2/3} ; \; j_g < j_{tr} \\ 1.5 \cdot 10^{-3} \left(\frac{k_m}{L}\right) \left(\frac{Pc_m j_g}{k_m g}\right)^{2/3} \left(\frac{j_{tr}}{j_g}\right)^{1/2} ; \; j_g \geq j_{tr} \end{cases} \tag{3}$$

where

$$j_{tr} = 4.3 \cdot 10^{-4} \frac{\sigma_m}{\mu_m}, \tag{4}$$

$$L = \sqrt{\frac{\sigma_m}{g\,(\rho_m - \rho_g)}}, \tag{5}$$

and j_g = superficial gas velocity, P = system pressure, μ = kinematic viscosity, σ = surface tension, c = specific heat, k = thermal conductivity, ρ = density, and g = gravitational acceleration. Subscripts m and g denote the melt and noncondensable gas phases, respectively. On the water side of the melt/water interface, film boiling heat transfer is assumed. The heat transfer coefficient is evaluated using the equation of Farmer et. al., (1),

$$h_w = A_* \left\{ \frac{k_e}{\delta_g} + h_{rad} \right\} + h_{entr} \tag{6}$$

where

$$h_{rad} = \eta\, \epsilon_m \left(T_m^2 + T_{sat}^2\right) \left(T_m + T_{sat}\right), \tag{7}$$

$$A_* = 1 + 4.5\, \frac{j_g}{U_\infty}, \tag{8}$$

and h_{entr} = heat transfer coefficient due to melt entrainment into water, η = Stefan-Boltzman constant, ϵ = radiation emissivity, δ_g = gas film thickness, U_∞ = sparging gas bubble terminal rise velocity (4), and subscript e denotes properties of the vapor/noncondensable gas film mixture. The expressions for δ_g, h_{entr}, and k_e are lengthy and are omitted here for the purposes of brevity; these expressions are provided in Reference (1). Note that the entrainment heat transfer coefficient, h_{entr}, is set equal to zero when Eq. 6 is used to evaluate Eq. 1. Although this term acts to augment the overall heat transfer coefficient (<1% for oxide melts (1)), it is not included in the local energy balance from which the interfacial temperature is evaluated, due to the fact that the local heat transfer characteristics across the gas film leading to incipient crust growth are governed by conduction and radiation. Based on the same reasoning, the dimensionless interfacial area enhancement, A_*, is set equal to 1 when Eq. 6 is used to evaluate Eq. 1.

The mechanical stability of an incipient crust formed at the melt/water interface will depend upon a variety of factors which may include fracture strength of the core/concrete mixture, thermal conductivity of the crust material, and degree of melt agitation induced by sparging concrete decomposition gases. Farmer et. al., (5) presented a model for the critical superficial gas velocity to preclude stable crust formation at the interface between a molten pool and water overlayer when the interfacial heat transfer occurs by film boiling. The model development and validation against experiment data is described in Reference (5). The solution for the critical gas velocity is given as,

$$j_c = \frac{.445\, R\, h_m\, (T_m - T_f)}{\delta_c\, \rho_{cr}\, \Delta e_{cr} \left\{ \frac{k_{cr}\, (T_f - T_{sat})}{\delta_c\, h_m (T_m - T_f)}\, \ln \left[\frac{1}{1 - \xi} \right] - 1 \right\}}, \tag{9}$$

where

$$\xi = \frac{h_m\, h_w\, (T_m - T_f)\, \delta_c}{k_{cr} \left(h_w\, (T_f - T_{sat}) - h_m\, (T_m - T_f) \right)}, \tag{10}$$

$$\delta_c = .69 \left[\frac{R^3\, (\rho_m - \rho_g)\, g}{\sigma_y} \right]^{1/2}, \tag{11}$$

and R = gas bubble radius sparging melt, σ_y = crust fracture stress, and Δe_{cr} = crust latent heat of fusion. Subscript cr denotes properties of the crust material. Note from denominator of Eqs. 9-10 that the condition $h_w\, (T_f - T_{sat}) > h_m\, (T_m - T_f)$ must be satisfied to obtain a physically realistic solution from this model. This requirement is identical to the thermal stability criterion, viz. Eq. 2. Thus, in addition to Eq. 2, the condition

$$j_g < j_c, \tag{12}$$

must be satisfied for sustained crust growth to occur at the melt/water interface. Above these two limits, the melt is envisioned to undergo bulk cooldown, with the melt/water heat transfer coefficient given through Eqs. 6-8. The appropriate temperature difference driving the upward heat transfer for this

case is $T_I - T_{sat}$, where T_I is evaluated through Eq. 1. When the thermal condition for incipient crust formation is satisfied (Eq. 2), two potential melt freezing modes may be observed, depending upon the pool sparging rate: (i) $j_g \geq j_c$, where crust segments are periodically broken up and mixed into the bulk melt, or (ii) $j_g < j_c$, where sustained crust growth occurs at the melt surface. These two cases are treated sequentially.

For situations in which $j_g \geq j_c$, periodic crust formation occurs at the melt surface, but pool agitation forces are sufficient to preclude sustained growth. Neglecting the decay heat source over these intermittent growth cycles, then the crust growth rate equation is of the form,

$$\rho_{cr}\,\Delta e_{cr}\,\frac{d\delta}{dt} = k_{cr}\,\frac{(T_f - T_I)}{\delta} - h_m\,(T - T_f), \tag{13}$$

where the crust upper surface temperature T_I, is given through the following energy balance at the crust/water interface,

$$k_{cr}\,\frac{(T_f - T_I)}{\delta} = h_w\,(T_I - T_{sat}). \tag{14}$$

Using Eq. 14 to eliminate T_I from Eq. 13 and integrating the resultant expression subject to $\delta\,(t = 0) = 0$ yields

$$\delta + \frac{k_{cr}}{h_m}\,\frac{(T_f - T_{sat})}{(T_m - T_f)}\,\ln\left[1 - \frac{\xi\delta}{\delta_c}\right] + \frac{h_m\,(T_m - T_f)}{\rho_{cr}\,\Delta e_{cr}}\,t_b = 0. \tag{15}$$

Equation 15 provides the local crust depth at the time at which the crust is broken up due to pool agitation forces t_b. Consistent with the development of Eq. 9 (5), t_b is assumed to correspond to the local bubble arrival time as given by Blottner's correlation (6), $t_b = .445\ R/j_g$. Given the intermittent crust depth from Eq. 15, the crust upper surface temperature, T_I, is evaluated from Eq. 14. The melt/water heat flux is then evaluated as $h_w(T_I - T_{sat})$, where h_w is evaluated through Eqs. 6-8.

For situations in which $j_g < j_c$, sustained crust growth at the melt/water interface will occur. Assuming (i) heat transfer through the crust is conduction limited (i.e., no heat transfer augmentation via water ingression is considered), and (ii) the heat transfer process is quasi-steady, then the conservation of

energy equation in the crust is of the form,

$$k_c \frac{\partial^2 T}{\partial x^2} + \rho_c \dot{q} = 0 \tag{16}$$

where $\dot{q}$ = crust decay heat level (W/kg). The boundary conditions on Eq. 16 at x = 0 (i.e., melt side of crust) are of the form

$$T(x = 0) = T_f \tag{17}$$

$$- k_{cr} \frac{\partial T}{\partial x}\Big|_{x=0} = h_m \left[T_m - T(x = 0)\right]. \tag{18}$$

Integration of Eq. 16 subject to Eqs. 17-18 yields the following solution for the crust temperature profile,

$$T(x) = - \frac{\rho_{cr} \dot{q}\, x^2}{2k_{cr}} - \frac{h_m (T_m - T_f)}{k_{cr}} x + T_f. \tag{19}$$

The crust thickness is then determined from an energy balance at $x = \delta$ (i.e., water side of crust),

$$- k_{cr} \frac{\partial T}{\partial x}\Big|_{x=\delta} = h_w \left[T\ (x=\delta) - T_{sat}\right], \tag{20}$$

which yields,

$$h_w \left[T\ (x=\delta) - T_{sat}\right] = h_m (T_m - T_f) + \rho_{cr} \dot{q} \delta. \tag{21}$$

Substitution for T $(x=\delta)$ from Eq. 19 into the above expression produces a quadratic equation for δ, the solution of which is

$$\delta = - \frac{h_m (T_m - T_f)}{\rho_{cr} q} + \sqrt{\left[\frac{h_m (T_m - T_f)}{\rho_{cr} q}\right]^2 + 2\, k_{cr} \frac{\left[T_f - T\ (x=\delta)\right]}{\rho_{cr} q}}\ . \tag{22}$$

Eqs. 21-22 constitute two equations in two unknowns for $T(x=\delta)$ and δ. The top heat flux from the coherent MCCI zone is then given by $h_m (T_m - T_f)$, whereas the cumulative heat flux from the MCCI zone plus crust is given by the left or right hand sides of Eq. 21.

For cases in which sustained crust formation occurs, the appropriate form of h_m

will most likely depend on the lateral distribution of "vent holes", or "fissures", through which concrete decomposition gases pass to the atmosphere. If the fissure spacing is fairly small (say on the order of the Laplace constant, L, defined in Eq. 5, which is ~5 mm for oxidic corium), then venting of decomposition gases will occur locally. In this situation, the heat transfer mechanism will be dominated by bubble agitation, for which Eq. 3 applicable. It is worth nothing, however, that if the fissure spacing is fairly large (>> L), then local voided regions may periodically form between the coherent melt zone and crust as the decomposition gases accumulate and flow to the vent sites. In this case, radiation heat transfer will play a significant role in determining the thermal loading on the crust lower surface. For the purposes of this work, this affect is neglected, and h_m is assumed to be given by Eq. 3.

According to Eq. 21, the cumulative heat flux to be extracted at the crust upper surface consists of decay heat within the crust plus heat convected to the crust underside from the melt. Thus, nucleate, transition, or film boiling heat transfer regimes may be encountered, depending upon where the cumulative heat flux lies with respect to the minimum film boiling and critical heat fluxes. Heat transfer in the nucleate boiling regime is calculated with Rohsenow's correlation (7). The crust upper surface is expected to be characterized by some degree of surface roughness. The associated surface area enhancement is expected to augment the boiling heat transfer over that which would be observed on a smooth surface. This tendency has been observed in the CWTI reactor material experiments (8, 9), as well as other experiments (10, 11). For definiteness, it is assumed that Rohsenow's heat transfer correlation (7) is augmented by a factor of 3 to characterize the surface roughness. The critical heat flux (CHF) is evaluated using the correlation of Ivey and Morris (12), which accounts for bulk coolant subcooling. The crust upper surface temperature at which CHF occurs is determined by setting the CHF expression equal to h_w ($T(x = \delta) - T_{sat}$), where h_w is given by the modified version of Rohsenow's correlation, and solving for $T(x = \delta)$. The minimum film boiling temperature is evaluated using Henry's correlation (13), which accounts for coolant subcooling and properties of the surface material. The heat transfer coefficient in the film boiling regime is calculated using Eq. 6 with h_{entr} set equal to zero (i.e., no melt entrainment into overlying water when crust is present), and the dimensionless surface area enhancement, A_*, fixed at a value of three to characterize surface roughness as

described above. The minimum film boiling heat flux is then evaluated as $h_w \Delta T_{min}$, with ΔT_{min} given by Henry's correlation (13), and h_w is evaluated through Eq. 6 with the above assumptions incorporated.

As discussed previously, heat transfer from the crust upper surface is heat flux-controlled from the melt side, and therefore between CHF and the minimum film boiling heat flux the film, transition, or nucleate boiling regimes may be encountered. Transition boiling is not considered to be a plausible long-term heat transfer mechanism, owing to the highly unstable nature of this boiling process. Film boiling is assumed to be the initial heat transfer mechanism in this analysis, due to initially high melt temperatures. This boiling regime is assumed to persist as long as the heat flux is above the minimum film boiling heat flux; below this value, nucleate boiling is assumed. However, it is important to note the unstable nature of film boiling over irregular oxide surfaces (14), and the possibility exists for transition to nucleate boiling at heat fluxes significantly above that predicted by the current modeling approach. If water ingression through the crust is not significant, then from an overall energy extraction viewpoint, the assumption of film versus nucleate boiling is insignificant since the heat transfer from the MCCI zone will be determined by conditions on the melt side of the crust. However, a crust which is in nucleate boiling at its upper surface will thermally equilibrate at a greater thickness in comparison to the film boiling case due to lower surface temperature. Thus, if crust mechanical stability over large lateral length scales (e.g., reactor cavity) plays a significant role in coolability, then the actual boiling regime which is encountered becomes an important consideration.

MODEL APPLICATIONS

Based on the current model, the heat transfer behavior at the melt upper surface is closely linked to the melt pool thermalhydraulic conditions. Thus, to make predictions regarding the melt cooling regime and corresponding melt/water heat flux, both the melt temperature and gas sparging rate must be specified, in addition to material properties. To evaluate the sparging rate for a given melt temperature, quasi-steady downward heat transfer is assumed, for which the basemat ablation rate is given by the expression,

$$\rho_{cn}\, e_{dc,cn}\, \frac{d\delta_b}{dt} = h_b (T_m - T_b) \qquad (23)$$

where ρ_{cn} = concrete density, $e_{dc,cn}$ = concrete decomposition enthalpy, h_b = melt/concrete heat transfer coefficient, and T_b = bottom temperature boundary condition. The gas sparging rate is related to the basemat ablation rate through the equation

$$j_g = \frac{\chi_{up}\, \chi_g\, \rho_{cn}}{\rho_g} \frac{d\delta_b}{dt} \qquad (24)$$

where ρ_g = sparging gas density, χ_g = weight fraction of decomposition gases in concrete, and χ_{up} = fraction of decomposition gases released upwards during concrete ablation. Results of the ACE MCCI reactor material experiments (15, 16) indicate that a significant fraction (~50%) of decomposition gases migrate downwards into concrete during the ablation process. Thus, for the purposes of this analysis, χ_{up} is set equal to 0.5.

The bottom heat transfer coefficient is evaluated with Bradley's model (17), which is a modified version of Kutateladze's correlation (3) (i. e., Eq. 3 is multiplied by 0.29 to account for the thermal resistance of the slag layer formed at the melt/concrete interface). The sparging gas is assumed to consist of H_2O and CO_2 (i.e., reduction of these gases by metals present in the melt is not considered). The gas densities are calculated using the ideal gas law evaluated at the particular melt temperature. Note that this assumption will influence the predictions since incomplete heating of gas bubbles as the bubbles ascend through the melt will lower the sparging rate for a given ablation rate, and therefore increase the melt temperature range over which crust formation occurs.

For the purposes of this study, the following melt thermal properties are assumed: k_m = 3.0 W/m•K, ρ_m = 7000 kg/m^3, C_m = 500 J/kg•K, μ_m = .01 kg/m•s, ϵ_m = 0.8, and σ_m = 0.6 N/m. Properties of the crust material are specified as: k_{cr} = 1.0 W/m•k, ρ_{cr} = 8000 kg/m^3, Δe_{ls} = 250 kJ/kg, and σ_y = 20 MPa. The concrete type is assumed to be limestone/common sand, for which ρ_{cn} = 2400 kg/m^3, $e_{dc,cn}$ = 2.5 MJ/kg, and χ_g = 0.27 (0.06 H_2O and 0.21 CO_2). The concrete decomposition temperature, T_{dc}, is taken equal to 1500 K. The calculations are performed at atmospheric pressure for which T_{sat} = 373 K. A representative coolant subcooling of 40 K is assumed. The surface/coolant constant, C_{sf}, in Rohsenow's correlation (7) is taken equal to 0.02, which is the reported value for water over stainless steel (note that the top crust surface temperature in the nucleate boiling regime

is insensitive to this parameter).

The melt/water heat flux, melt/concrete heat flux, critical gas velocity, concrete decomposition gas velocity, crust depth, and crust/melt surface temperature predictions are shown in Figures 2-3 for assumed melt freezing temperature of 1700 K and the bottom temperature boundary condition taken equal to T_{dc}. The low freezing temperature assumption is consistent with scenarios in which water is added atop the MCCI after significant concrete erosion has taken place, thereby causing a reduction in T_f due to entrainment of concrete decomposition products into the melt. This assumption is consistent with the experiment conditions of the MACE Scoping Test (2). Consistent with the experiment technique, the calculation was performed assuming no decay heat in the crust.

The upward heat flux during the scoping test decreased gradually from ~600 kW/m^2 at 20 minutes past water addition, down to ~150 kW/m^2 at 70 minutes after water was added. During this period, the average melt temperature decreased gradually from ~1900-2000 K down to ~1800 K. (Note that the initial melt/water heat flux was ~3.5 MW/m^2 over the first four minutes, but due to asymmetry in the ablation front, melt temperature data is not available until 20 minutes after water addition). From Figure 2, the predicted upward heat fluxes for T_m = 1900-2000 K

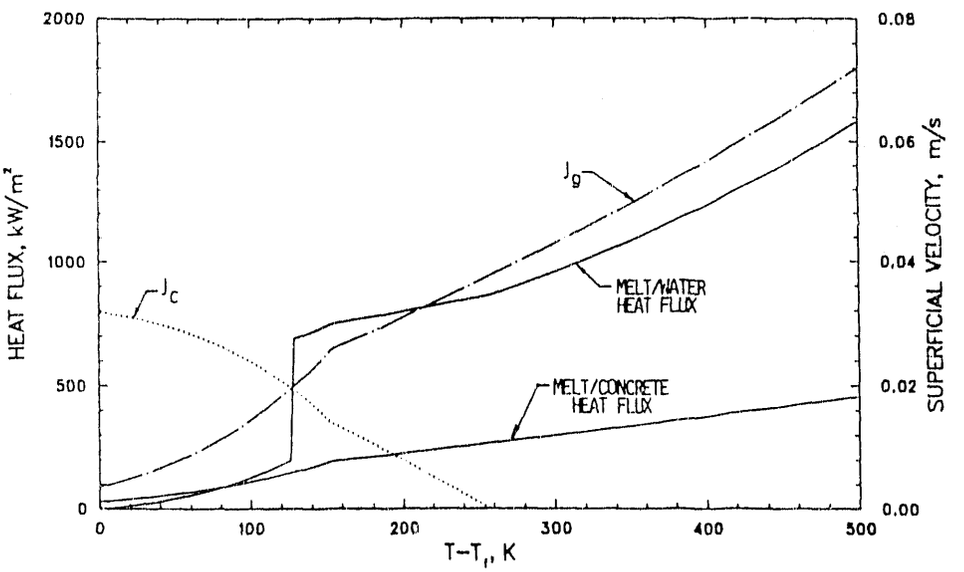

Figure 2. Predicted Melt/Water Heat Flux and Critical Gas Velocity Versus Melt Superheat for the Case T_f = 1700 K, T_b = 1500 K, and $\dot{q}$ = 0.

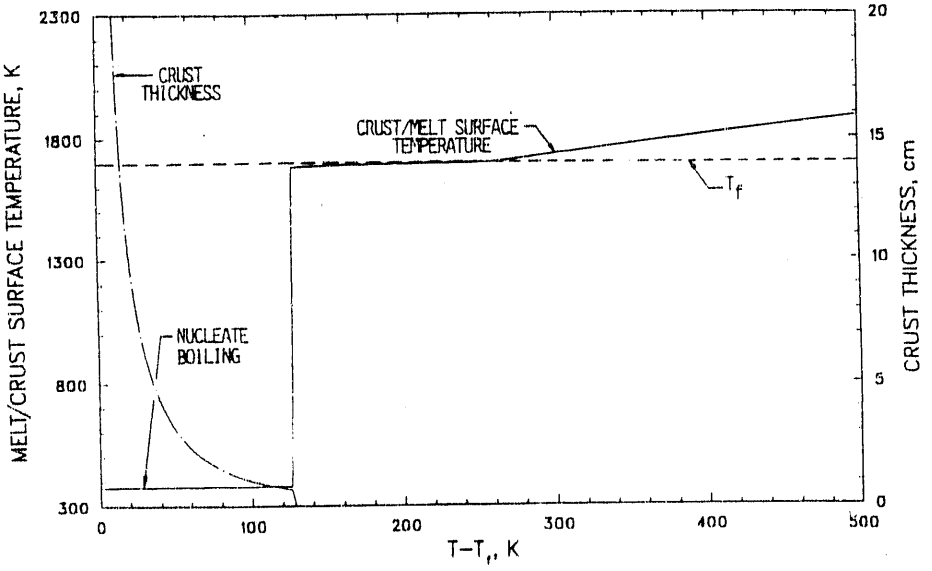

Figure 3. Predicted Crust Thickness and Melt/Crust Surface Temperature for the Case T_f = 1700 K, T_b = 1500 K, and $\dot{q}$ = 0.

are 700-950 kW/m^2, and the predicted flux for T_m = 1800 K is 120 kW/m^2. Thus, the predicted heat fluxes bracket those observed during the scoping test. Note from Figs. 2-3 that the heat transfer behavior is predicted to change from purely bulk cooldown to bulk cooling with periodic crust formation at T_m = 1960 K, at which point $T_I = T_f$, but $j_g > j_c$. Additionally, the heat transfer characteristics change from bulk cooldown with periodic crust formation to a stable crust configuration at T_m = 1830 K, at which point $j_g = j_c$. The heat flux at the bifurcation point in the latter case is predicted to drop from 680 kW/m^2 to 200 kW/m^2, reflecting the formation of a stable interfacial crust. A similar transformation was observed in the scoping test at t = 25 minutes, where the heat flux dropped from ~600 kW/m^2 to ~350 kW/m^2. The melt temperature measurements at this time ranged from 1800-2000 K. However, the change in heat flux was coincidental with an observed melt eruption from the surface (2). It is not clear whether the reduction in heat flux at this point is representative of a change in melt cooling regimes or an artifact of the eruptive event. As shown in Fig. 3, heat transfer from the crust upper surface is predicted to occur by nucleate boiling (i.e., $T_I - T_{sat}$ = 373 K). This is due to the fact that the crust thermal loading, $h_m(T_m - T_f)$, does not exceed the minimum film boiling heat flux over the melt temperature range where a stable crust configuration is

predicted. There is no experiment evidence to either confirm or deny this prediction. Also from Fig. 3, the crust depth at the end of the scoping test (T_m ~1800 K) is predicted to be 1.3 cm. Posttest examinations indicated crust depths ranging form 1.9-2.5 cm.

To assess the affects of decay heat in the crust on the scoping test predictions, the above calculation was repeated with $\dot{q}$ = 350 W/kg (i.e., PWR decay heat level at ~2 hrs into the accident progression). The results are shown in Figs. 4-5. In the range $j_g > j_c$, the predictions are identical. For $j_g < j_c$, the upwards heat flux increases from 90 kW/m^2 at T_m = 1700 K (reflecting decay heat in the crust) up to 210 kW/m^2 at $j = j_c$ (T_m = 1830 K). These heat fluxes may be compared with the predicted values of 0-200 kW/m^2 over the same temperature range for the experiment (see Fig. 2). The predicted crust depth for the reactor case varies from 3.1 cm at $T_m = T_f$ (again, reflecting decay heat in the crust) down to 0.0 cm at $j_g = j_c$. At T_m =1800 K (i.e., melt temperature at end of scoping test), the crust depth is found to be 0.9 cm, which may be compared with the previously cited prediction of 1.3 cm for the scoping test.

SUMMARY AND CONCLUSIONS

Modeling improvements have been incorporated into the CORQUENCH mechanistic melt/water heat transfer model such that the model is now capable of treating both the bulk cooldown and crust-limited heat transfer phases of the quench process. The approach is to define thermal and mechanical thresholds for incipient crust formation at the melt upper surface. Above these thresholds, the melt undergoes bulk cooling due to radiation dominated film boiling heat transfer across the agitated (i.e., area enhanced) melt/water interface. Below these thresholds, heat transfer from the MCCI zone is limited by conduction across an interstitial crust. The revised model is compared with the results of the MACE scoping test; the predicted melt/water heat flux and crust depth show reasonable agreement with the experiment data.

ACKNOWLEDGEMENTS

This work is sponsored by the Advanced Containment Experiments (ACE) International Consortium through the Electric Power Research Institute, Contract

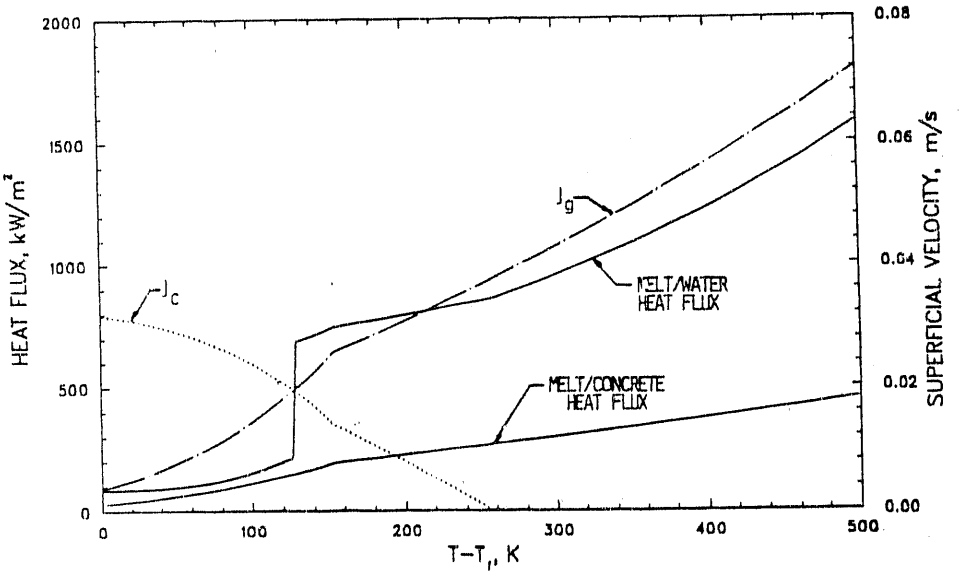

Figure 4. Predicted Melt/Water Heat Flux and Critical Gas Velocity Versus Melt Superheat for the Case T_f = 1700 K, T_b = 1500 K, and $\dot{q}$ = 350 W/kg.

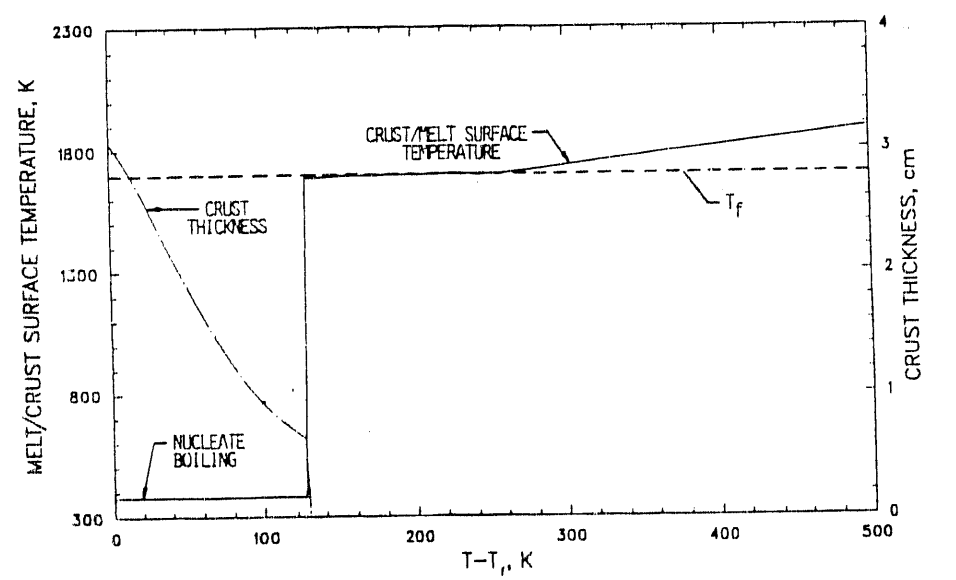

Figure 5. Predicted Crust Thickness and Melt/Crust Surface Temperature for the Case T_f = 1700 K, T_b = 1500 K, and $\dot{q}$ = 350 W/kg.

No. RP 3047-08. The EPRI Program coordinator is B. R. Sehgal. The manuscript was patiently typed by L. J. Ondracek.

REFERENCES

1. M. T. Farmer, J. J. Sienicki, and B. W. Spencer, "CORQUENCH: A Model for Gas Sparging Enhanced, Melt-Water, Film Boiling, Heat Transfer," ANS Winter Meeting on the Thermal Hydraulics of Severe Accidents, Washington, D.C., November 11-15, 1990.

2. B. W. Spencer, et. al., "MACE Scoping Test," MACE-TR-D03, June 1991.

3. S. S. Kutateladze and I. G. Malenkov, "Boiling and Bubbling Heat Transfer Under the Conditions of Free and Forced Convection," 6th Int. Heat Transfer Conf., Toronto, 1978.

4. F. N. Peebles and H. J. Garber, "Study on the Motion of Gas Bubbles in Liquids," Chem. Engr. Progr., Vol., 49, pp. 88-97, 1953.

5. M. T. Farmer, et. al., "Modeling and Database for Melt-Water Interfacial Heat Transfer," submitted to 2nd CSNI Specialist Meeting on Core-Debris Interactions, Karlsruhe, FRG, April 1-3, 1992.

6. F. G. Blottner, "Hydrodynamics and Heat Transfer Characteristic of Liquid Pool with Bubble Agitation," Sandia National Laboratory, SAND79-1132, NUREG/CR-0844, November 1979.

7. W. H. Rohsenow, "A Method of Correlating Heat Transfer Data for Surface Boiling of Liquidus," Trans. ASME, Vol. 74, pp. 969-976, 1952.

8. J. J. Sienicki and B. W. Spencer, "Analysis of Reactor Material Experiments on Corium-Water Thermal Interactions in Ex-Vessel Geometry," Proc. International Meeting on Light Water Reactor Severe Accident Evaluation, Vol. 2, pp. 12.1-1 - 12.1-8, 1983.

9. B. W. Spencer, L. M. McUmber, and J. J. Sienicki, "Results and Analysis of Reactor-Material Experiments on Ex-Vessel Corium Quench and Dispersal," Proc. 5th International Meeting on thermal Nuclear Reactor Safety, Vol. 2, pp. 1079-1089, 1984.

10. D. S. Jung, J. E. S. Venart, and A. C. M. Sousa, "Effects of Enhanced Surfaces and Surface Orientation on Nucleate and Film Boiling Heat Transfer in R-11," International J. Heat Mass Transfer, Vol. 30, pp. 2627-2639, 1987.

11. S. K. R. Chowdhury and R. H. S. Winterton, "Surface Effects on Pool Boiling," International J. Heat Mass Transfer, Vol. 28, pp. 181-1889, 1985.

12. H. J. Ivey and D. J. Morris, "On the Relevance of the Vapor-Liquid Exchange Mechanisms for Subcooled Boiling Heat Transfer at High Pressure," AEEW-R127, 1962.

13. R. E. Henry, "A Correlation for the Minimum Film Boiling Temperature," AIChE Symp. Ser., Vol. 70, pp. 81-90, 1974.

14. F. Moreaux, J. C. Chevrier, and G. Beck, "Destabilization of Film Boiling by Means of a Thermal Resistance," Int. J. Multiphase Flow, Vol. 2, pp. 183-180, 1975.

15. D. H. Thompson, et. al.., "Thermal Hydraulic Aspects of the Large-Scale Integral MCCI Lists in the ACE Program," submitted to 2nd CSNI Specialist Meeting on Core-Debris Interactions," Karlsruhe, FRG, April 1-3, 1992.

16. J. K. Fink, et. al., "Aerosol Released During Large-Scale Integral MCCI Tests in the ACE Program," submitted to 2nd CSNI Specialist Meeting on Core-Debris Interactions," Karlsruhe, FRG, April 1-3, 1992.

17. D. R. Bradley, "Modeling of Heat Transfer Between Core Debris and Concrete, "ANS Proceedings 1988 National Heat Transfer Conference, Houston, TX, July 24-27, 1988.

DISCLAIMER

END

DATE FILMED

5/14/92